

1 **Comparison of the degradations of diphenamid by homogeneous** 2 **photolysis and heterogeneous photocatalysis in aqueous solution**

3
4
5 Hai-chao Liang^a, Xiang-zhong Li^{a,*}, Yin-hua Yang^b, Kong-hung Sze^{b,**}

6 ^a *Department of Civil and Structural Engineering, The Hong Kong Polytechnic University,*
7 *Hong Kong, China*

8 ^b *Department of Chemistry, The University of Hong Kong, Hong Kong, China*

9 **Corresponding author. Tel.: +852 2766 6016; Fax: +852 2334 6389; E-mail address:*

10 cexzli@polyu.edu.hk

11 ***Second Corresponding author: Tel.: +852 2859 7915; Fax: +852 2857 1586; E-mail address:*

12 khsze@hkucc.hku.hk

13
14 **Abstract**

15 In this work, the homogeneous and heterogeneous degradations of diphenamid (DPA) in
16 aqueous solution were conducted by direct photolysis with UVC (254 nm) and by
17 photocatalysis with TiO₂/UVA (350 nm), and the experimental results were compared. It
18 was found that the homogeneous photolysis by UVC irradiation alone was quite efficient to
19 degrade DPA up to 100% after 360 min, but was very inefficient to mineralize its
20 intermediates in terms of dissolved organic carbon reduction of only 8%. In contrast, the
21 heterogeneous photocatalysis with TiO₂/UVA showed relatively a lower degree of DPA
22 degradation (51%), but a higher degree of its mineralization (11%) after 360 min. These
23 results reveal that the photocatalysis process has relatively poor selectivity to degrade
24 different compounds including various intermediates from the DPA degradation, which is
25 beneficial to its mineralization. In addition, over 20 intermediates were identified by LC-MS
26 and ¹H-NMR analyses. Based on the identified intermediates, the reaction mechanisms and
27 the detailed pathways of the DPA degradation by photolysis and photocatalysis were
28 proposed, and are presented in this paper.

30 *Keywords:* Diphenamid; Herbicide; NMR; Photolysis; Photocatalysis

31

32

33 **1. Introduction**

34

35 Diphenamid (DPA) as a pre-emergent herbicide is widely employed for control of annual
36 grasses and broadleaf weeds in tomato, potato, peanut, and soybean plants (Schultz and
37 Tweedy, 1972; Sirons et al., 1981). This substance does enter the environment under normal
38 use or through inappropriate disposal and is harmful to aquatic organisms. Therefore, the
39 investigation of remediation treatments of polluted waters containing trace amounts of
40 herbicides is of environmental interests.

41 In the past decades, research on the photochemical degradation of DPA in aqueous
42 solution has progressed quickly because of the high efficiency of mineralization under the
43 mild operating conditions (Rosen, 1967; Schultz and Tweedy, 1972; Rahman et al., 2003).
44 For example, Rosen (1967) studied the homogeneous photodegradation of DPA by UV and
45 sunlight irradiation, but the mechanism and the major products from DPA degradation were
46 not well identified. Rahman et al. (2003) investigated the photocatalytic degradation of DPA
47 in aqueous P25 TiO₂ suspension under the illumination of a medium pressure mercury lamp.
48 Although they identified five intermediates using a GC-MS technique and suggested a brief
49 pathway of the DPA degradation, the five products identified in their study were not
50 sufficient enough to buildup a thorough pathway delineating the photocatalytic degradation
51 of DPA due to the complexity of the DPA molecular structure. Furthermore, the medium
52 pressure mercury lamp used in their experiment offers a broad band of light emission from
53 200 to 600 nm, thus resulting in both types of processes, homogeneous photolysis and
54 heterogeneous photocatalysis, to possibly occur in the DPA degradation. In short, the
55 literatures reported previously did not supply a clear clarification of the photochemical

56 reactions for the degradation of DPA pollutants in water. Therefore, in order to better
57 understand the difference of DPA degradation by homogeneous photolysis and heterogeneous
58 photocatalysis, two sets of experiments for DPA degradation in aqueous solution by direct
59 photolysis with UVC and photocatalysis with TiO₂/UVA were conducted in this study. In
60 which, the reaction mechanisms and pathways of DPA degradation by direct photolysis and
61 photocatalysis were proposed based on over 20 intermediates identified by the combination
62 of ¹H-NMR and LC-MS analyses.

63

64 **2. Experimental**

65 *2.1. Materials*

66 DPA chemical (99.9%) was purchased from Aldrich Chemical Company. Self-prepared
67 TiO₂ films as reported before (Liang and Li, 2009) were used as photocatalysts. 0.5 M HCl and
68 0.5 M NaOH solutions were used to adjust the solution pH. Other chemicals such as CDCl₃ and
69 CH₃CN (Aldrich) were used without further purification. Deionized distilled water was used
70 throughout the experiments.

71

72 *2.2. Experimental setup and procedure*

73 A UV-photoreactor system consists of a quartz reactor, an external UV light source, one
74 piece of TiO₂ film with an area of 3 cm², and 25 mL of aqueous DPA solution. The UV lamp
75 was placed perpendicularly on the top of the reactor and the distance between the lamp and
76 the surface of solutions was ~6 cm (see Supplemental Material (SM), Fig. SM-1). In order to
77 compare the effect of UV wavelengths on the photochemical behavior of direct photolysis
78 and photocatalysis, DPA solutions were irradiated with different UV lamps: (a) UVC region,
79 using a G8T5 germicidal lamp with a maximum at 254 nm (Sankyo Denki Co. Ltd., Japan);
80 (b) UVA region, using a F8T5/BL-B black light blue lamp with a wavelength range of 318-

81 400 nm and its main emission at 350 nm (Hitachi, Japan). Both UV lamps had an equivalent
82 power consumption of 8 W and the corresponding light intensity detected in the experiment
83 was $8.02 \times 10^{-4} \text{ W cm}^{-2}$ for UVC and $1.01 \times 10^{-3} \text{ W cm}^{-2}$ for UVA, respectively. Prior to
84 photocatalytic reaction, the DPA solution of 20 mg L^{-1} was magnetically stirred in the dark
85 for 60 min in order to achieve adsorption/desorption equilibrium. Then the DPA
86 concentration ($\sim 19.2 \text{ mg L}^{-1}$) in the bulk solution at this time was used as an initial value. All
87 reactions were performed at room temperature of $\sim 21 \text{ }^\circ\text{C}$. During the photocatalytic reaction,
88 the samples were collected from the solution at different intervals.

89

90 2.3. Chemical analysis

91 The DPA concentration was determined by HPLC (Finnigan SpectraSYSTEM P4000)
92 consisting of a Pinnacle II C18 reverse-phase column ($5 \mu\text{m}$, $4.6 \text{ mm} \times 250 \text{ mm}$) and a UV
93 detector (UV 6000LP) at 254 nm. The mobile phase consisted of acetonitrile/water (v:v = 3:2)
94 with 0.5 vol% acetic acid/phosphoric acid, and flowed at 1.0 mL min^{-1} . In order to identify
95 the organic reaction intermediate species, combination of LC-MS and $^1\text{H-NMR}$ analyses
96 were employed. All one-dimensional and two-dimensional (2D) $^1\text{H-NMR}$ spectra were
97 recorded at ambient temperature using a NMR spectrometer (Bruker Avance 600 MHz)
98 equipped with a tick carboxypeptidase inhibitor cryoprobe. To avoid missing out any
99 intermediates at a low concentration during the NMR analysis, it is necessary to extract the
100 organic substrates in the final water samples with chloroform (HPLC grade) before the NMR
101 detection. Although the DPA solutions with an initial concentration of 20 mg L^{-1} were used in
102 the experiments to determine the kinetic reaction rate constants (k) of photolysis and
103 photocatalysis reactions, the higher concentration of DPA at 130 mg L^{-1} was used in the
104 experiments to identify the intermediates by $^1\text{H-NMR}$ analysis. In the meantime, an ion trap
105 mass spectrometer (Finnigan LCQTM DUO) coupled to LC-MS was also used to further verify

106 the reaction intermediates through electrospray ionization (ESI). The ESI probe was installed
107 with sheath and auxiliary gasses at 60 and 20 units, respectively. The mass spectrometer was
108 operated in the positive/negative ion mode in the m/z 50-400 range for LC-MS and LC-
109 MS/MS. The MS conditions were set at capillary temperature = 250 °C, voltage = 46 V and
110 spray voltage = 4.5 kV.

111 Dissolved organic carbon (DOC) concentration was determined by a total organic carbon
112 (TOC) analyzer (TOC-5000A, Shimadzu, Japan) equipped with an auto-sampler (ASI-5000).
113 O₂ as a carrier gas was used in the detecting system. In this analysis, organic carbon = total
114 carbon (TC) – inorganic carbon (IC). Under the acidic condition, all inorganic carbon was
115 converted to CO₂ and measured. Prior to the TOC analysis, two standard solutions, potassium
116 hydrogen phthalate (KOOCC₆H₄COOH) solutions in the range of 10-100 mg L⁻¹ and
117 sodium carbonate (Na₂CO₃) solutions of 1-10 mg L⁻¹, were used to calibrate TC and IC
118 concentrations respectively. The minimum acceptable correlation coefficient (R^2) was 0.9991
119 and the detection limit of the method was 0.1 mg L⁻¹.

120

121 **3. Results and discussion**

122

123 *3.1. Direct photolysis and photocatalysis of DPA in aqueous solutions*

124 The photodecay of DPA by UV light radiation with and without catalyst is thought to
125 follow the pseudo-first-order reaction with respect to the DPA concentration (Rahman et al.,
126 2003). In this study, the semi-log graphs of the DPA degradation by photolysis and
127 photocatalysis versus irradiation time yield straight lines, indicating the pseudo-first-order
128 reaction kinetics. The reaction rate constants (k) were evaluated from the experimental data
129 by the linear regression. In all cases R^2 values are higher than 0.97, indicating that the
130 exponential model can well describe the kinetics for DPA degradation in both processes.

131 DOC was also monitored to compare the degree of DPA mineralization in both processes at
132 different pH.

133

134 [Table 1]

135

136 The two sets of experiments in aqueous DPA solutions without TiO₂ film at pH 3.5, 7.2
137 and 9.6 were first conducted under UVC and UVA illumination, respectively for 360 min.
138 The experimental results are shown in Table 1. It can be seen that while the direct photolysis
139 with UVA showed almost no reduction of DPA after 360 min at three pH values, the direct
140 photolysis with UVC showed that, DPA was degraded by 100% after 360 min at pH 3.5, 7.2
141 and 9.6, but the corresponding DOC was only reduced by 11, 8 and 9%, respectively. These
142 results indicate that DPA cannot be degraded by direct photolysis under UVA illumination
143 (350 nm) because of its main light absorption at ~260 nm, but it can be excited by UVC light
144 (254 nm) and then quickly degraded through direct electron transfer reaction. However, the
145 direct UVC-photolysis had poor mineralization when the DOC removal is considered to
146 reflect the degree of mineralization. The effect of pH on DPA degradation indicated that DPA
147 was degraded from fast to slow in an order of pH 3.5 > 9.6 > 7.2. It can be attributed to the
148 unique ionic states of DPA under acidic and alkaline conditions. Both the acidic and alkaline
149 conditions favored UV absorption by DPA (Fig. SM-2), resulting in faster homolytic or
150 heterolytic breakages in the DPA molecules. With the further photolysis reaction, some acidic
151 products were formed from the DPA degradation.

152

153 To conduct a photocatalysis reaction without direct photolysis, aqueous DPA solution in
154 presence of TiO₂ film was irradiated by the UVA light in the wavelength range of 318-400
155 nm under different pH conditions and the experimental results are also presented in Table 1.

156 It can be seen that at pH 3.5, DPA was degraded by 63% and DOC was reduced by 13% after
157 360 min whereas at pH 9.6, DPA was degraded by 42% and DOC by 8%. These results
158 indicate that DPA can be degraded by the photocatalysis with TiO₂/UVA, but more slowly
159 than that by the photolysis with UVC. Furthermore, it was found that under acidic and neutral
160 conditions, the DOC removal by the photocatalysis (13 and 11%, respectively) was higher
161 than that by photolysis (11 and 8%, respectively). These results might indicate that
162 photocatalysis process has poor selectivity for degrading different intermediates from the
163 DPA degradation, which is beneficial to DPA mineralization, especially under the acidic
164 condition, while the direct photolysis showed the relatively lower DOC removals.

165

166 *3.2. Mechanism of homogeneous and heterogeneous DPA degradation*

167 TiO₂-based photocatalysis is well known to produce •OH radicals in water, through the
168 interface oxidation of hydroxide anions or water molecules adsorbed on the semiconductor
169 surface by the holes photogenerated in the valence band of semiconductor. The •OH radicals
170 produced by TiO₂ are the powerful oxidizing species and can initiate the degradation of
171 aromatic compounds by direct attack to the aromatic rings, leading to the formation of
172 hydroxylated intermediate species (as shown in the later discussion). At sufficient contact
173 time and proper operation conditions, it is practically possible to mineralize the target
174 pollutant to CO₂ and H₂O. This property results in good mineralization for the TiO₂/UVA
175 photocatalysis. However, it should be noted that the photocatalytic process mainly occurs on
176 the photocatalyst surface, but not in the bulk solution; in other words, the photocatalytic
177 process depends on the adsorption and diffusion of DPA/intermediate molecules on the TiO₂
178 surface, thus leading to a slow rate of DPA degradation.

179 In contrast, the mechanism of the direct UVC-induced photolysis ($\lambda = 254$ nm) is based
180 on the fact that the chemical species undergo the homogeneous reactions in solution, by

181 which molecules are broken down to smaller molecules as a result of photodecomposition of
182 the excited organic compounds. The sequence of events that could occur during a particular
183 DPA photolytic decomposition is summarized below.



189
190 Here Eq. 1 involves the excitation of DPA, in which the photo-excited state of DPA^* takes
191 one-electron from the ground state of DPA molecule to produce radical anion $\text{DPA}\cdot^-$.
192 Subsequent reaction can either undergo thermal deexcitation (Eq. 2) via recombination of
193 radical ions or photodecomposition to produce intermediate I_{uv} (Eq. 3). Some intermediates
194 I_{uv} can also absorb UV light to produce excited state intermediate I_{uv}^* as shown in Eq. 4,
195 further undergoing the decomposition towards final products step by step (Eq. 5), but some
196 cannot when energy absorbed by intermediate molecules directly from UV light is not
197 enough to cause the bond scission. The formation of resistant intermediates just explains the
198 fact that generally direct photolysis has a lower degree of mineralization than that of
199 photocatalysis with TiO_2 .

200

201

202 3.3. Identification of intermediates

203 Both the LC-MS and $^1\text{H-NMR}$ analyses were used to detect the intermediates. It should
204 be noted that the NMR technique can avoid the escaping of some polar intermediates and
205 positional isomers generally occurring in the MS analysis alone. Table 2 and Table SM-1
206 summarized the analytical results along with the proposed structures for the detected

207 byproducts, in which 21 intermediate products were identified according to the mass ion
208 peaks from MS spectra and the characteristic proton patterns from ¹H-NMR spectra. Three
209 principal groups of intermediate products were identified in both homogeneous and
210 heterogeneous degradation processes: (i) products 1–4 from the reactions relevant to only the
211 *N*-methyl oxidation or replacement; (ii) products 5–12 from the reactions of the
212 hydroxylation of the aromatic ring; and (iii) products 13–21 from the *N*-demethylation,
213 oxidation and ring opening. The intermediate products 1-7 were listed in Table 2 and other
214 products 8-21 were shown in Table SM-1.

215

216 [Table 2]

217

218 In this paper, both positive and negative ion full-scan mode experiments over the mass
219 range from *m/z* 50 to 400 were used to determine the *m/z* of the individual components
220 related to DPA and its degradation products, as shown in Fig. 1. For comparison, the
221 fragmentation pattern obtained from photolysis (Fig. 1a) was analogous to that of TiO₂-
222 photocatalysis (Fig. 1b), for the most part, and supports the assigned structure (see Table 2).
223 For example, the major ions with *m/z* 256 and 272, corresponding to mono- and bi-
224 hydroxylation respectively, were both observed in spectra (a) and (b). The major ion with *m/z*
225 333 is due to the couple of fragments of $-\text{CH}(\text{C}_6\text{H}_5)_2$, whereas the minor ion (*m/z* 196) should
226 be interpreted as arising from cleavage of the bond between the carbonyl group and the *N*-
227 dimethyl group. By analogy, formation of fragment ions at *m/z* 105 and 123 in MS spectra of
228 byproducts 18 and 19 can be rationalized. The structures of the identified fragments (*m/z* 287,
229 301, 316, 366) are shown in Table SM-1. It should be pointed out that this type of
230 fragmentation was already observed for iodosulfuron degradation by Sleiman et al. (2006).

231 [Fig. 1]

232

233 Some of $^1\text{H-NMR}$ spectra were used to further determine the chemical structures of the
234 degradation products of DPA as shown in Fig. 2. Figure 2a depicts the *p*-, *o*- and *m*- regions
235 (5.35–5.70 ppm) of the 2D-COSY spectra of DPA solutions after the irradiation by direct
236 UVC photolysis for 1 h and by TiO_2/UVA photocatalysis for 24 h. This is the time at which
237 the DPA degradation exceeded 50% and the concentrations of its products were sufficient to
238 be observed clearly in the NMR analysis. 2D-COSY analysis was conducted in our study
239 because in a COSY spectrum the coupling interaction is generally allowed to identify which
240 protons couple to each other. From Fig. 2a, it is interesting to find that for the DPA molecule
241 there is the existence of a strong cross peak that corresponds to the chemical shifts of both
242 protons, in which the horizontal line from the spot at 3.00 ppm corresponds to the methyl
243 protons while the vertical line drawn from the spot at 5.58 ppm corresponds to the methine
244 protons. The presence of this cross peak, which correlates the methyl protons and methine
245 protons, confirms that (1) such COSY method can detect the long-range coupling interaction
246 that extends to five bonds (Pavia et al., 2001) and (2) the methyl and methine groups must be
247 present simultaneously in DPA molecules. Besides this, other four types of cross peaks,
248 similar to the nature of DPA molecule, were also observed in this COSY spectrum. They are
249 nonequivalent, probably owing to the nuclear magnetization effect of the methyl neighbor
250 group. Therefore, combining the specific proton information with corresponding MS data,
251 the four intermediates can be identified as compounds 1–4 arising from oxidation or removal
252 of terminal N-methyl group in DPA molecule, simultaneously appearing in the UVC
253 photolysis and TiO_2/UVA photocatalysis processes.

254

255 [Fig. 2]

256

257 The second category of products includes different phenolic compounds resulting from
258 the hydroxylation of benzene ring during the UVC and TiO₂/UVA processes. The different
259 intermediates reflect the difference in the reaction mechanisms of two processes: the
260 homogeneous degradation of DPA by photolysis is dependent upon the bond strength of
261 DPA/intermediate molecules and their energy absorbing ability, while the heterogeneous
262 degradation of DPA by photocatalysis is mainly affected by the attack of •OH radicals.
263 Among these products, compounds 5, 6 and 7 are positional isomers and they were
264 discriminated by ¹H-NMR rather than MS analysis. Since the chemical shift of ortho-proton
265 of most phenolic compounds is 6.0–7.0 ppm in many literatures (Limiroli et al., 1996; Es-Safi
266 et al., 2000), the evolution of main products belonging to this group is represented on the
267 NMR spectra in the region of 6.0–7.2 ppm, as shown in Fig. 2b. It can be clearly observed
268 that some strong proton signals occurred in the spectrum (C). According to the mass of 256
269 m/z, compounds 5, 6 and 7 would be recognized with the monosubstitution by OH in the
270 para-, ortho- and meta-position, respectively. While compounds 6 and 7 had the same
271 concentration level, compound 5 showed the higher concentration level of about 4.5 times
272 than that of compounds 6 and 7. This result indicates that compound 5 is a major
273 hydroxylated product from the DPA degradation by TiO₂/UVA due to the regioselective attack
274 of •OH. This can be explained by the electron density of the benzene carbon sites and the
275 steric hindering effects of the benzene ring substituents (–CHCON(CH₃)₂), where the para-
276 position is more nucleophilic and accessible than the other two positions at ortho and meta
277 orientation. In contrast, spectrum (B) in Fig. 2b shows very low proton signals of compounds
278 5 and 6, indicating that the hydroxylation of benzene ring in DPA structure is not a
279 dominating process by direct photolysis under UVC irradiation. It should be noted that the
280 different chemical shifts of compounds 5 and 6 in both spectra (B) and (C) resulted from the
281 effect of different final pH, such as pH 6.47 in the direct photolysis but pH 5.56 in the

282 photocatalysis. Water samples were extracted with chloroform to concentrate the organics for
283 further analysis. As a result, it was identified that some multi-hydroxylated products
284 (compounds 8–12, $n_{\text{OH}} = 2\text{--}5$) appeared in the TiO_2/UVA process but not in the UVC process
285 when corroborating with their mass ion peaks in LC-MS spectra. NMR spectra of organic
286 extracts are not presented in this paper.

287

288 *3.4. Degradation pathways*

289 The results in Table 2 reflect a fact that there are different pathways between the DPA
290 degradations in photolytic and photocatalytic processes due to the evolution of different
291 principal intermediates. Figure 3 illustrates the proposed pathways of DPA degradation by
292 UVC irradiation alone, which may not include every possible reactions but covering the main
293 approaches confirmed by the identified products. The major decay pathways include N-
294 methyl oxidation, scission of the N-CO or C-CO bond, dimerization and ring opening. The
295 results have been compared to those from previous research with analogous degradation
296 mechanisms such as tyrosine, phenylthioacetic acid and phenylurea derivatives photolysis
297 (Jin et al., 1995; Filipiak et al., 2006), which are similar to our findings. For specific
298 intermediates, compound 1, arising from N-methyl oxidation, is considered to be the major
299 primary intermediate in the process (see Fig. 2). The oxidation of terminal methyl group
300 involves an intramolecular hydrogen bond between N-methyl and carbonyl groups in the
301 excited state (Jirkovský et al., 1997), and then reacts with dissolved molecular oxygen to
302 form formylated product $[-\text{N}(\text{CH}_3)\text{CHO}]$. This indicates a key role played by the
303 photoexcited oxygen species and the formation of the formylated product by oxidation of the
304 N-methyl group was the major reaction observed. The subsequent reduction and further
305 oxidation of compound 1 gave rise to form compounds 2 and 3, in which compound 3 easily
306 underwent the decarboxylation to yield compound 4 via photo-kolbe reactions (Krautler and

307 Bard, 1978). The evolution profiles of compounds 1–4 in Fig. 2 offer useful information in
308 supporting this pathway. On the other hand, no products that obviously come from further
309 oxidation of the second N-methyl group were detected in our experiments. Despite
310 hydroxylated products 5 and 6 were detected, the fact that they only existed at trace levels
311 and implied that hydroxylation of aromatic ring was not a minor pathway in the UVC
312 photolysis process.

313 [Fig. 3]

314

315 Direct irradiation leads to the promotion of a molecule from the ground state to an excited
316 state. Such excited states can undergo homolysis or heterolysis, among other processes. It is
317 known that a 254 nm photon has an equivalence of 4.89 eV, which should be enough
318 energetic to produce homolytic or heterolytic breakages in the molecules (Litter, 2005).
319 Therefore, it can be expected that further photolysis bond scission could take place, followed
320 by radical recombination or H-/(HO-) abstracting from water solvent. For instance, scission
321 of the N-CO bond leads to yield the diphenylacetic acid (compound 15) while scission of the
322 C-CO bond gives benzhydrol (compound 16) as a major intermediate and a trace amount of
323 compound 13. The cleavage of compound 16 can produce small molecules such as phenol
324 (compound 17) and benzaldehyde (compound 18), where benzaldehyde can easily undergo
325 further oxidation to form secondary intermediate benzoic acid (compound 19) while phenol
326 trends to undergoing the ring opening to form product 20. The observed product 20,
327 belonging to an aliphatic polyene acid, can be successively transformed into product 21 and
328 finally to CO₂ and H₂O. A similar pathway for phenol degradation by photolysis was
329 proposed by Jin et al. (1995).

330 In the heterogeneous photocatalysis process with TiO₂/UVA, hydroxylation reactions of
331 the aromatic ring are the most frequently observed primary reaction due to the attack of •OH

332 (Amine-Khodja et al., 2002). Similarly, these reactions were proposed in Fig. 4, which are
333 significantly different from that of DPA photolytic process. First, isomers 5-7 were identified
334 as the phenolic compounds monosubstituted by OH in para-, ortho- and meta-position,
335 respectively, suggesting that the aromatic ring has an electron-donating effect, due to the
336 electrophilicity of hydroxyl radicals. It is interesting that isomer 5 shows the highest
337 concentration level, following by isomers 6 and 7. These results indicate that the
338 monohydroxylation of aromatic ring with corresponding H abstraction by \bullet OH attack not
339 only is a major reaction step in the photocatalytic process but also takes place regioselectively
340 on the aromatic ring. By further attack of \bullet OH, its subsequent reaction with oxidizing species
341 yielded the multihydroxylated intermediates (compounds 8–12), such as di-, tri-, tetra- and
342 quint-substitution phenolics. However, the low concentrations of these products reveal that
343 the multihydroxylation reaction might occur just as a minor route in the photocatalytic
344 degradation of DPA. Further oxidation by \bullet OH attack can result in the benzene ring opening
345 to yield maleic acid (compound 21). The ring opening is possibly due to the formation of a
346 hydroxycyclohexadienyl radical in photocatalysis process (e.g. radical B in Fig. 4), confirmed
347 by Aceituno et al. (2002). Besides this, both oxidation of N-methyl groups and N-
348 demethylation on the urea moiety of DPA were also proposed, as shown in Fig. 5. These
349 reactions were conducted through attack by hydroxyl radicals and reaction with oxygen.
350 Although the compounds 1-4 were found in both photolysis and photocatalysis, their
351 evolution underwent different reactions by bond scission and \bullet OH attack, respectively.

352 [Fig. 4]

353 [Fig. 5]

354

355 **4. Conclusions**

356 The experiments demonstrated that DPA degradation by direct photolysis with UVC

357 proceeded quickly, but its further mineralization was difficult, while the DPA degradation by
358 photocatalysis with TiO₂/UVA proceeded more slowly, but achieved a higher extent of
359 mineralization. Using both the LC–MS and ¹H–NMR analyses together is a powerful
360 approach to identify more than 20 intermediates from the DPA degradation. The analytical
361 results indicate that two processes undergo some similar reactions such as the oxidation of N-
362 methyl group of side chain, but also undergo some different approaches. For example, the
363 hydroxylation of aromatic ring was observed as a major way in the photocatalytic process
364 while it is a minor one in the direct photolytic process. This fundamental research about the
365 mechanism of photolytic and photocatalytic reaction provides essential knowledge with
366 potential to further develop a best process for aqueous DPA degradation in water treatment.

367

368 **Acknowledgement**

369 The authors wish to acknowledge the support of the Research Committee of The Hong Kong
370 Polytechnic University in providing a PhD scholarship for H. C. Liang.

371 **Supplemental Material**

372

373 Supplementary data associated with this article can be found, in the online version, at xxxxxx.

374

375 **References**

376 Aceituno, M., Stalikas, C.D., Lunar, L., Rubio, S., Pérez-Bendito, D., 2002. H₂O₂/TiO₂

377 photocatalytic oxidation of metol: identification of intermediates and reaction pathways.

378 Water Res. 36, 3582–3592.

379 Amine-Khodja, A., Lavédrine, B., Richard, C., Sehili, T., 2002. Photocatalytic degradation of

380 metoxuron in aqueous suspensions of TiO₂: analytical and kinetic studies. Int. J.

381 Photoenergy 4, 147–151.

382 Es-Safi, N.E., Guernevé, C.L., Cheynier, V., Moutounet, M., 2000. New phenolic
383 compounds obtained by evolution of (+)-catechin and glyoxylic acid in hydroalcoholic
384 medium. *Tetrahedron Lett.* 41, 1917–1921.

385 Filipiak, P., Hug, G.L., Marciniak, B., 2006. Photochemistry of carboxylic acids containing
386 the phenyl and thioether groups: steady-state and laser flash photolysis studies. *J.*
387 *Photochem. Photobiol. A* 177, 295–306.

388 Jin, F., Leitich, J., Sonntag, C.V., 1995. The photolysis ($\lambda = 254$ nm) of tyrosine in aqueous
389 solutions in the absence and presence of oxygen: the reaction of tyrosine with singlet
390 oxygen. *J. Photochem. Photobiol. A* 92, 147-153.

391 Jirkovský, J., Faure, V., Boule, P., 1997. Photolysis of diuron. *Pestic. Sci.* 50, 42-52.

392 Krautler, B., Bard, A.J., 1978. Heterogeneous photocatalytic synthesis of methane from
393 acetic acid - new Kolbe reaction pathway. *J. Am. Chem. Soc.* 100, 2239-2240.

394 Liang, H.C., Li, X.Z., 2009. Effects of structure of anodic TiO₂ nanotube arrays on
395 photocatalytic activity for the degradation of 2,3-dichlorophenol in aqueous solution. *J.*
396 *Hazard. Mater.* 162, 1415-1422.

397 Limiroli, R., Consonni, R., Ranalli, A., Bianchi, G., Zetta, L., 1996. ¹H NMR study of
398 phenolics in the vegetation water of three cultivars of *olea europaea*: similarities and
399 differences. *J. Agr. Food Chem.* 44, 2040-2048.

400 Litter, M.I., 2005. Introduction to photochemical advanced oxidation processes for water
401 treatment. *The Handbook of Environmental Chemistry, Vol. 2, Part M, Environmental*
402 *Photochemistry Part II.* Springer-Verlag, Berlin.

403 Pavia, D.L., Lampman, G.M., Kriz, G.S., 2001. Introduction to Spectroscopy: A Guide for
404 Students of Organic Chemistry 3rd ed., Brooks/Cole, , Singapore, pp. 266-267.

405 Rahman, M.A., Muneer, M., Bahnemann, D., 2003. Photocatalysed degradation of a
406 herbicide derivatives, diphenamid in aqueous suspension of titanium dioxide. *J. Adv.*
407 *Oxid. Technol.* 6, 100–108.

408 Rosen, J.D., 1967. The photolysis of diphenamid. *B. Environ. Contam. Tox.* 2, 349-354.

409 Schultz, D.P., Tweedy, B.G., 1972. The effect of light and humidity on absorption and
410 degradation of diphenamid in tomatoes. *J. Agr. Food Chem.* 20, 10-13.

411 Sirons, G.J., Zilkey, B.F., Frank, R., Paik, N.J., 1981. Residues of diphenamid and its
412 phytotoxic metabolite in flue-cured tobacco. *J. Agr. Food Chem.* 29, 661-664.

413 Sleiman, M., Ferronato, C., Fenet, B., Baudot, R., Jaber, F., Chovelon, J.M., 2006.
414 Development of HPLC/ESI-MS and HPLC/1H NMR methods for the identification of
415 photocatalytic degradation products of iodosulfuron. *Anal. Chem.* 78, 2957-2966.

417

418

419 **List of figure captions**

420 Fig. 1. The full-scan mass spectra in the m/z 50-400 range for the degradation of DPA by
421 photolysis (a) and TiO₂-photocatalysis (b).

422 Fig. 2. ¹H-NMR analysis of DPA degradation by UVC and TiO₂/UVA treatments: (a) 2D-
423 COSY spectra of aqueous DPA solutions, in which the proton signals of methine group
424 in DPA and compounds 1–4 were marked; (b) Relevant region of 1D ¹H-NMR spectra
425 of DPA and its hydroxylation products 5, 6 and 7.

426 Fig. 3. Proposed pathways of the DPA degradation by direct photolysis with UVC.

427 Fig. 4. Proposed pathways of the DPA degradation by photocatalysis with TiO₂/UVA. Here,
428 R1 is p- or m-phenolic ring; R2 is 3,5-diphenolic ring; and R' includes benzene ring, R1,
429 and R2.

430 Fig. 5. Mechanism of oxidation of N-methyl group in DPA molecules by photocatalysis

432

433 Table 1. Effects of solution pH on DPA degradation efficiency, kinetic constants, correlation

434 coefficients and DOC removal by different systems after 360 min reaction. Here, $C_0 =$ 435 20 mg L^{-1} .

System	DPA decay ($1-C/C_0$, %)			$k^a \times 10^{-3} (\text{min}^{-1})/R^2$			DOC removal (%)		
	pH 3.5	7.2	9.6	pH 3.5	7.2	9.6	pH 3.5	7.2	9.6
UVC	100	100	100	32/0.999	19/0.979	24/0.998	11	8	9
UVA	– ^b	–	–	–	–	–	–	–	–
TiO ₂ /UVA	63	51	42	1.8/0.979	1.3/0.994	1.0/0.978	13	11	8

436 ^a - The pseudo-first order kinetic constant437 ^b - not detected.

438

439

440

441

442

443

444

445

446

447

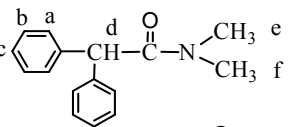
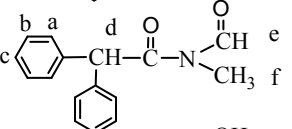
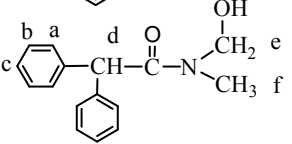
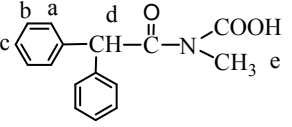
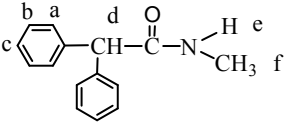
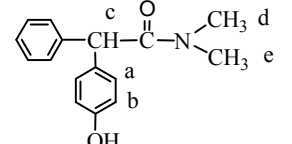
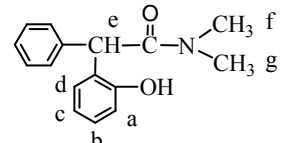
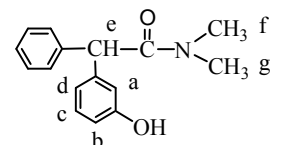
448

449

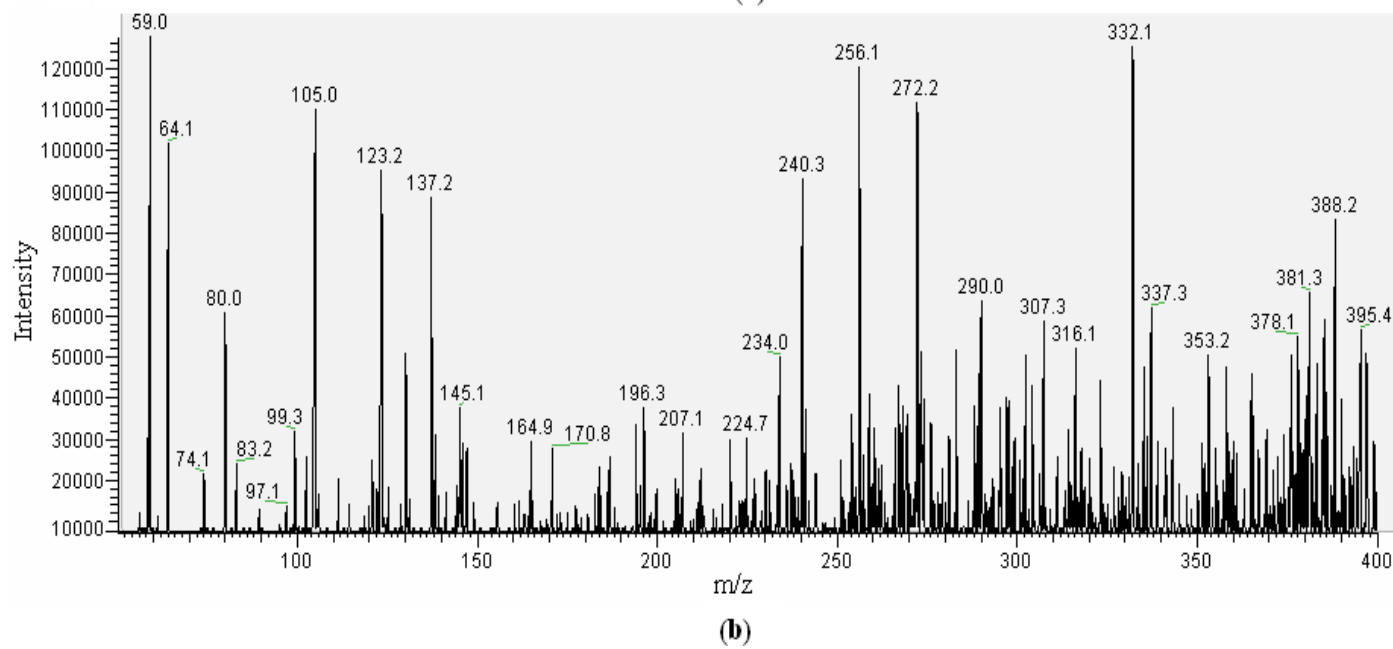
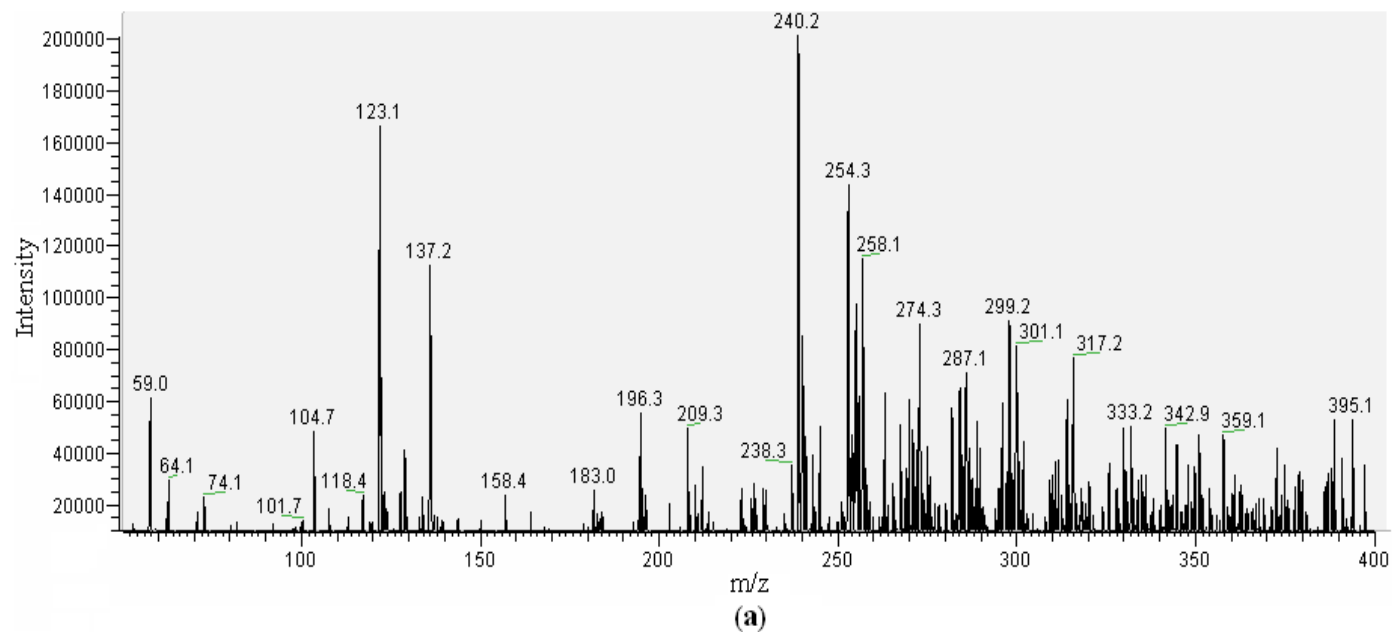
450

Table 2. Products resulting from the direct photolysed and photocatalysed degradation of DPA by MS and ¹H-NMR analysis.

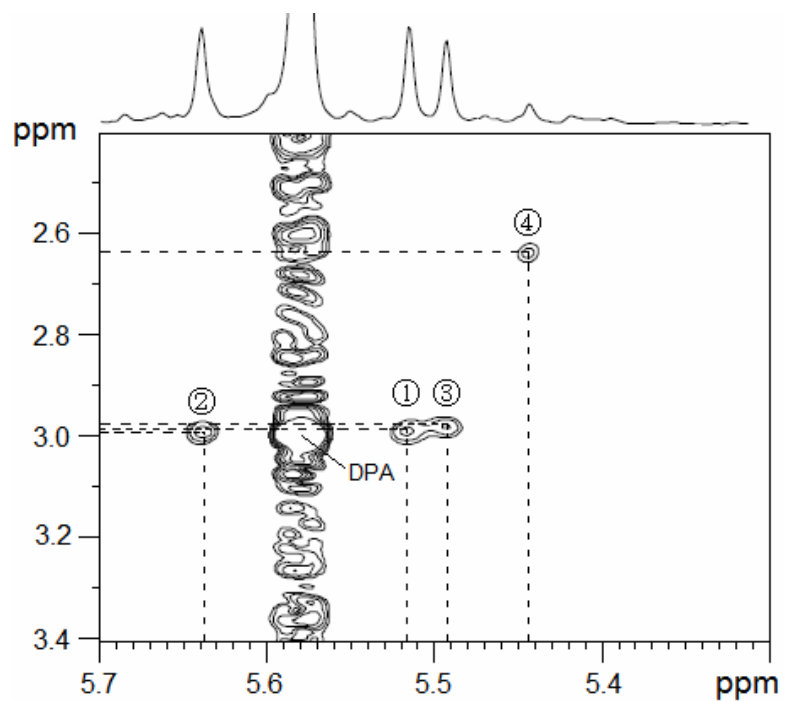
Other products 8-21 were shown in Table SM-1.

Compound No.	Structures ^(a)	MS data (m/z)	¹ H-NMR data (δ, multiplicity ^(b) , coupling constant)	Products of DPA degradation ^(c)	
				UVC	TiO ₂ /UVA
DPA		238 (M-H) ⁻ 240 (M+H) ⁺ 241 (M+2H) ⁺⁺	a: 7.22 (4H, d, <i>J</i> _{ab} = 8.56); b: 7.41 (4H, m); c: 7.35 (2H, t, <i>J</i> _{cb} = 7.18); d: 5.58 (1H, s); e: 3.04 (3H, s); f: 3.00 (3H, s)	+	+
1		251 (M+O-2H) ⁻⁻ 254 (M+O+H) ⁺ 255 (M+O+2H) ⁺⁺	a: 7.22 (4H, d, <i>J</i> _{ab} = 8.56); b: 7.41 (4H, m); c: 7.35 (2H, t, <i>J</i> _{cb} = 7.18); d: 5.52 (1H, s); e: 8.44 (1H, s); f: 3.11 (3H, s)	+	+
2		255 (M+O) 256 (M+O+H) ⁺ 258 (M+O+3H) ⁺⁺⁺	a: 7.22 (4H, d, <i>J</i> _{ab} = 8.56); b: 7.41 (4H, m); c: 7.35 (2H, t, <i>J</i> _{cb} = 7.18); d: 5.64 (1H, s); e: 5.89 (2H, s); f: 3.04 (3H, s)	+	+
3		268 (M+2O-H) ⁻ 270 (M+2O+H) ⁺ 271 (M+2O+2H) ⁺⁺	a: 7.22 (4H, d, <i>J</i> _{ab} = 8.56); b: 7.41 (4H, m); c: 7.35 (2H, t, <i>J</i> _{cb} = 7.18); d: 5.49 (1H, s); e: 3.08 (3H, s)	+	+
4		224 (M-CH ₂ -H) ⁻ 226 (M-CH ₂ +H) ⁺ 227 (M-CH ₂ +2H) ⁺⁺	a: 7.22 (4H, d, <i>J</i> _{ab} = 8.56); b: 7.41 (4H, m); c: 7.35 (2H, t, <i>J</i> _{cb} = 7.18); d: 5.43 (1H, s); e: 7.51 (H, m); f: 2.99 (3H, d, <i>J</i> _{fe} = 4.05)	+	+
5		254 (M+O-H) ⁻ 256 (M+O+H) ⁺ 257 (M+O+2H) ⁺⁺	a: 7.10 (2H, d, <i>J</i> _{ab} = 9.11); b: 6.88 (2H, d, <i>J</i> _{ba} = 9.09); c: 5.58 (1H, s); d: 3.04 (3H, s); e: 3.00 (3H, s)	trace	+
6		254 (M+O-H) ⁻ 256 (M+O+H) ⁺ 257 (M+O+2H) ⁺⁺	a: 6.91 (1H, d, <i>J</i> _{ab} = 8.79); b: 7.01 (1H, m); c: 7.01 (1H, m); d: 6.95 (1H, d, <i>J</i> _{dc} = 8.58); e: 5.58 (1H, s); f: 3.04 (3H, s); g: 3.00 (3H, s)	trace	+
7		254 (M+O-H) ⁻ 256 (M+O+H) ⁺ 257 (M+O+2H) ⁺⁺	a: 6.71 (1H, s); b: 6.78 (1H, d, <i>J</i> _{bc} = 9.75); c: 7.09 (1H, m); d: 6.84 (1H, d, <i>J</i> _{dc} = 9.50); e: 5.58 (1H, s); f: 3.04 (3H, s); g: 3.00 (3H, s)	trace	+

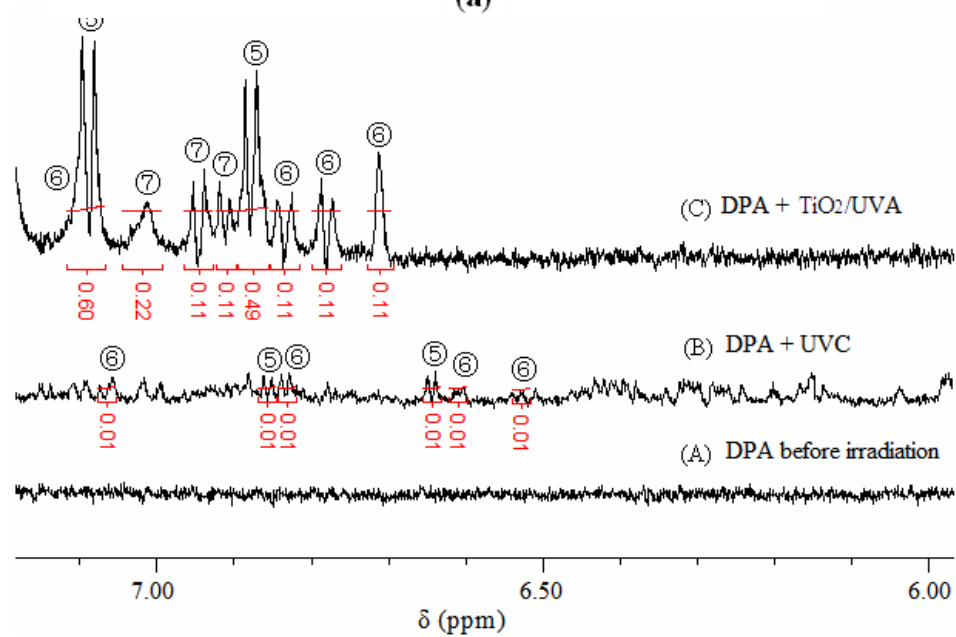
[Fig. 1]



[Fig. 2]



(a)



(b)

[Fig. 3]

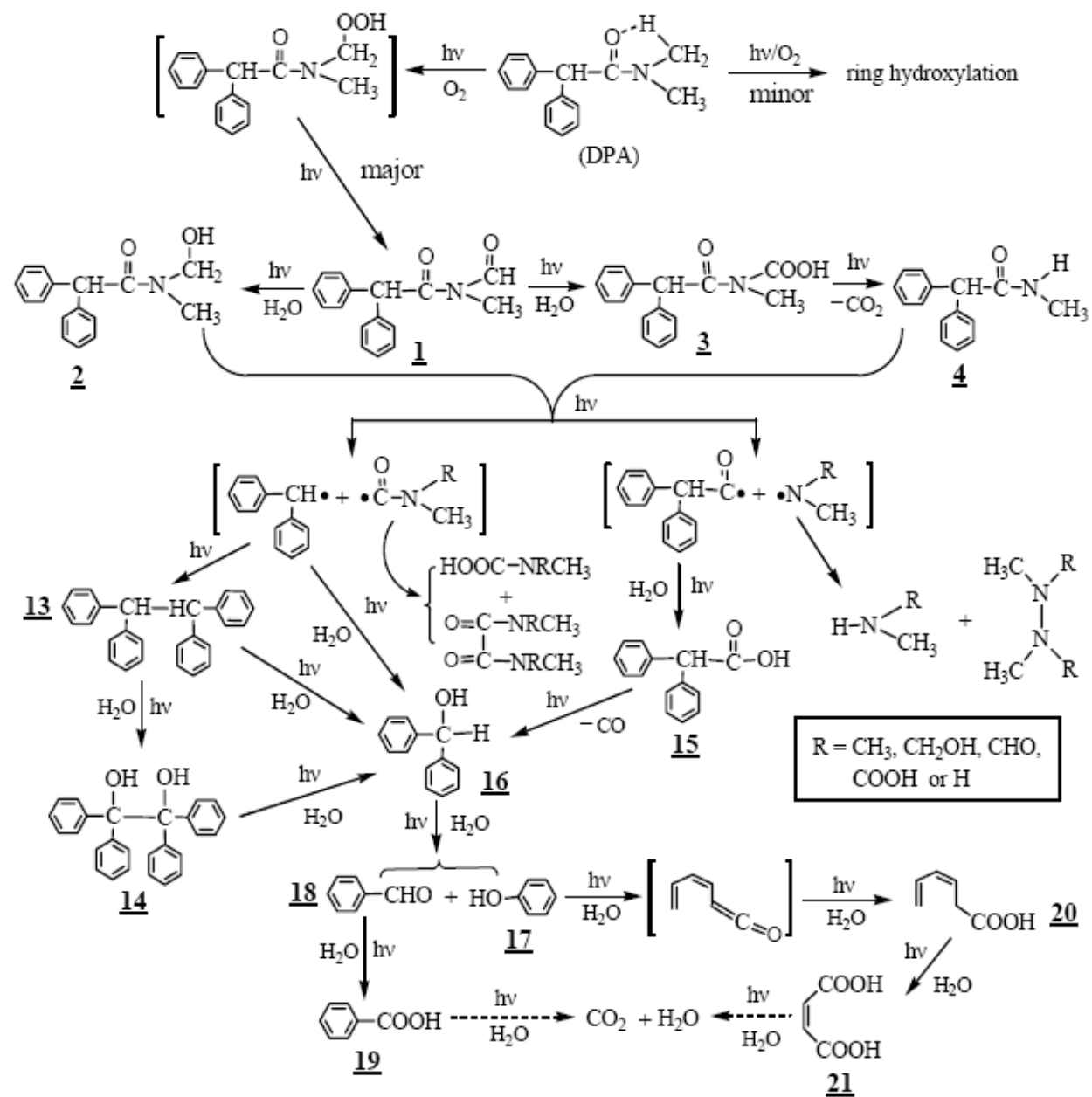


[Fig. 4]

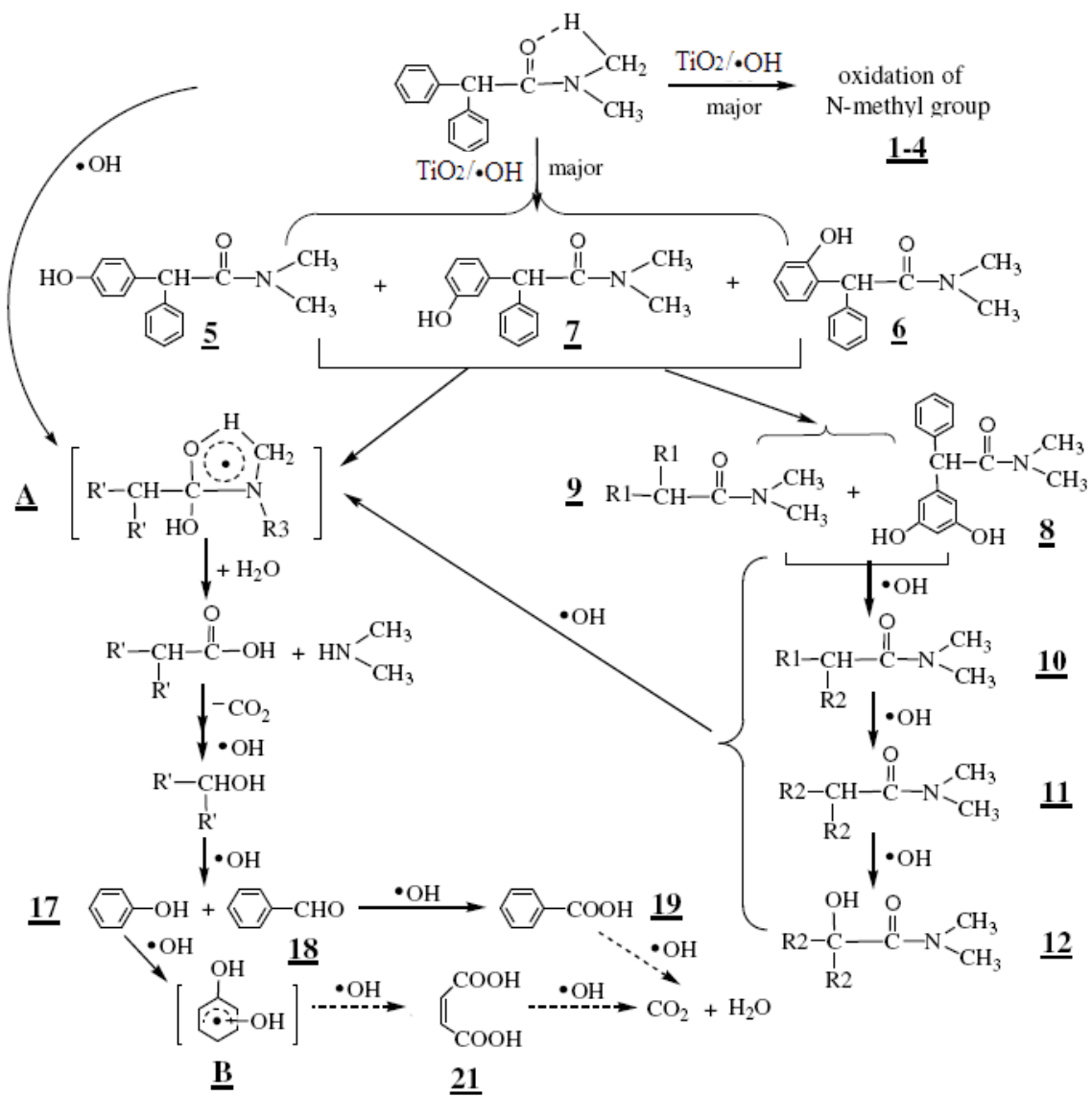
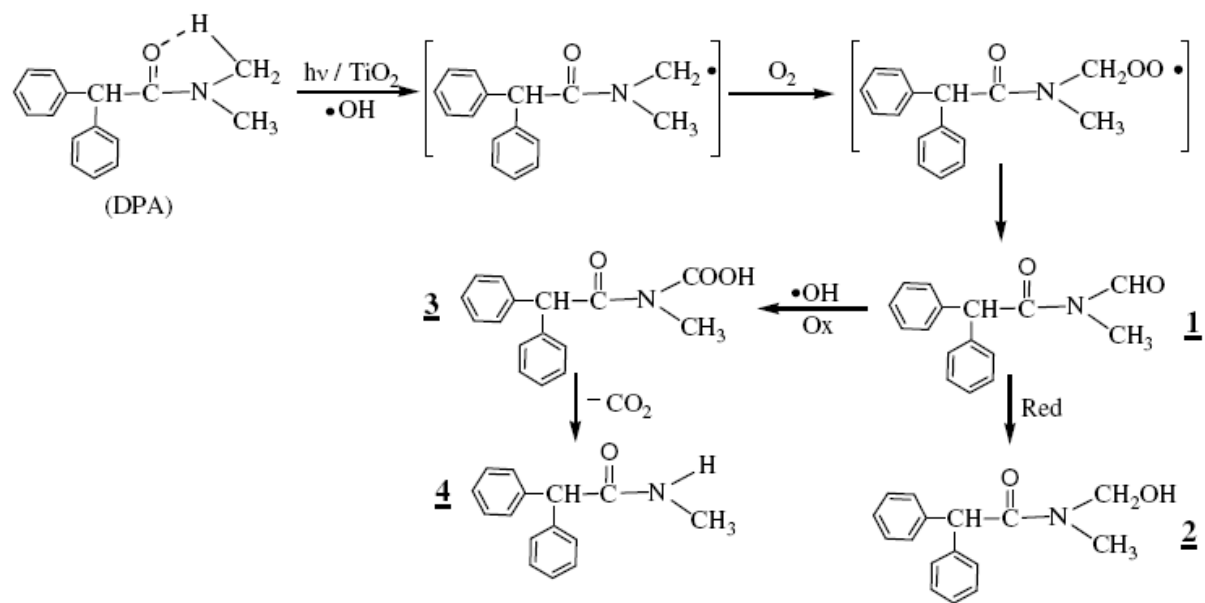


[Fig. 5]



Supplemental Material:

[Fig. SM-1] Diagram of the batch-scale photocatalytic-reactor.

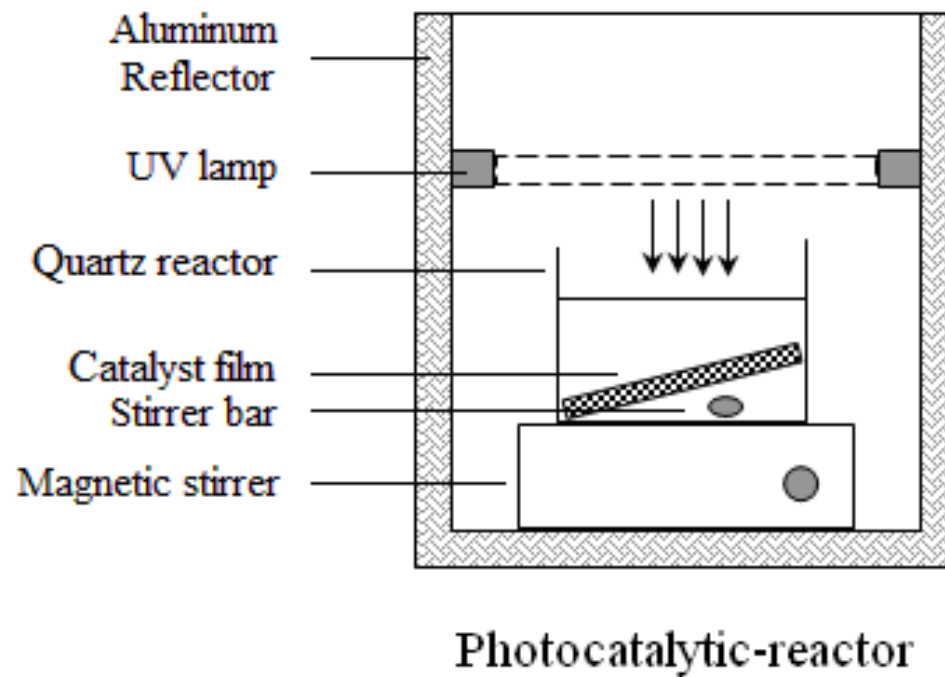
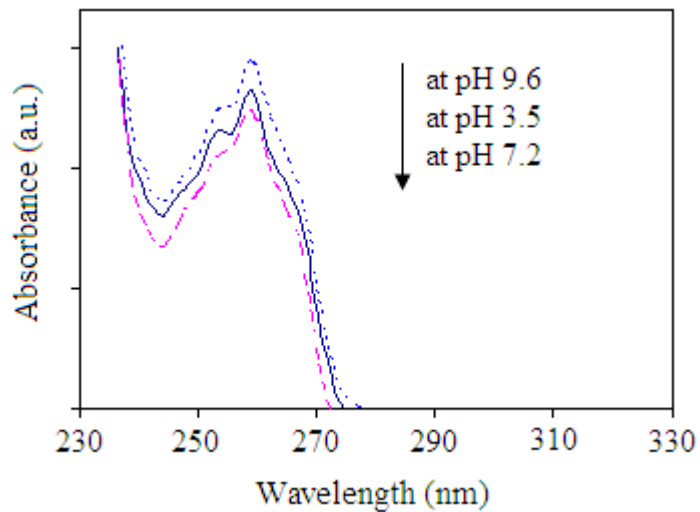


[Fig. SM-2] UV-visible spectra of aqueous DPA solutions at different pH media before irradiation.

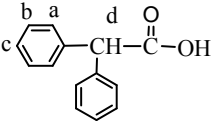
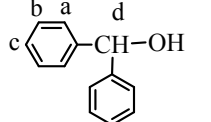
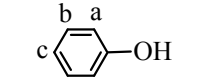
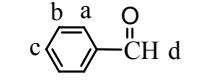
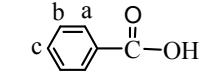
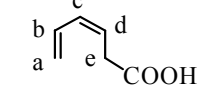
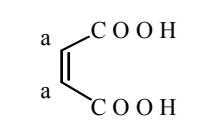


(The color figure is intended to be reproduced in black-and-white.)

Table SM-1. Products 8-12 resulting from the direct photolysed and TiO₂-photocatalysed degradation of DPA by MS and ¹H-NMR analysis.

Compound No.	Structures ^(a)	MS data (m/z)	¹ H-NMR data (δ, multiplicity ^(b) , coupling constant)	Products of DPA degradation ^(c)	
				UVC	TiO ₂ /UVA
8^(d)		272 (M+H) ⁺ 273 (M+2H) ⁺⁺ 274 (M+3H) ⁺⁺⁺	a: 6.63 (2H, s); b: 6.57 (1H, s); c: 5.58 (1H, s); d: 3.04 (3H, s); e: 3.00 (3H, s)	–	trace
9^(d)		272 (M+H) ⁺ 273 (M+2H) ⁺⁺ 274 (M+3H) ⁺⁺⁺	a: 5.58 (1H, s); b: 3.04 (3H, s); c: 3.00 (3H, s)	–	trace
10^(d)		285 (M-3H) ⁻⁻⁻ 288 (M+H) ⁺ 290 (M+3H) ⁺⁺⁺	a: 6.63 (2H, s); b: 6.57 (1H, s); c: 5.58 (1H, s); d: 3.04 (3H, s); e: 3.00 (3H, s)	–	trace
11^(d)		300 (M-3H) ⁻⁻⁻ 303 (M) 304 (M+H) ⁺ 306 (M+3H) ⁺⁺⁺	a: 6.63 (2H, s); b: 6.57 (1H, s); c: 5.58 (1H, s); d: 3.04 (3H, s); e: 3.00 (3H, s)	–	trace
12^(d)		316 (M-3H) ⁻⁻ 318 (M-H) ⁻ 322 (M+3H) ⁺⁺⁺ 323 (M+4H) ⁺⁺⁺⁺	a: 6.63 (2H, s); b: 6.57 (1H, s); c: 5.58 (1H, s); d: 3.04 (3H, s);	–	trace
13^(d)		332 (M-2H) ⁻⁻ 333 (M-H) ⁻ 336 (M+2H) ⁺⁺	a: 7.51(4H, d, J _{ab} = 8.22); b: 7.53 (4H, m); + c: 7.45 (2H, t, J _{cb} = 8.14); d: 4.89 (1H, s);	–	–
14^(d)		365 (M-H) 366 (M) 367 (M+H) ⁺	a: 7.49 (5H, s)	+	–

Table SM-1 (Continue)

Compound No.	Structures ^(a)	MS data (m/z)	¹ H-NMR data (δ , multiplicity ^(b) , coupling constant)	Products of DPA degradation ^(c)	
				UVC	TiO ₂ /UVA
15		211 (M-H) ⁻ 212 (M) 213 (M+H) ⁺	a: 7.22 (4H, d, J_{ab} = 8.56); b: 7.41 (4H, m); c: 7.35 (2H, t, J_{cb} = 7.18); d: 5.12 (1H, s);	+	+
16		183 (M-H) ⁻ 184 (M) 185 (M+H) ⁺	a: 7.39 (4H, d, J_{ab} = 8.02); b: 7.51 (4H, m); c: 7.47 (2H, t, J_{cb} = 8.81); d: 5.89 (1H, s);	+	+
17 ^(d)		93 (M-H) ⁻ 94 (M) 95 (M+H) ⁺	a: 6.85 (2H, d, J_{ab} = 6.54); b: 7.25 (2H, m); c: 6.99 (1H, t, J_{cb} = 7.55)	trace	trace
18		105 (M-H) ⁻	a: 7.89 (2H, d, J_{ab} = 9.24); b: 7.51 (2H, m); c: 7.74 (1H, t, J_{cb} = 8.31); d: 9.34 (1H, s);	+	+
19		121 (M-H) ⁻ 122 (M) 123 (M+H) ⁺	a: 8.16 (2H, d, J_{ab} = 9.20); b: 7.67 (2H, m); c: 7.49 (1H, t, J_{cb} = 8.12);	+	+
20 ^(d)		111 (M-H) ⁻ 112 (M) 113 (M+2H) ⁺⁺	a: 5.83 (2H, d, J_{ab} = 8.91); b: 6.15 (1H, m); c: 6.44 (1H, m); d: 5.97 (1H, m); e: 3.38 (2H, d, J_{ed} = 3.85);	+	-
21 ^(d)		115 (M-H) ⁻ 118 (M+2H) ⁺⁺	a: 6.36 (2H, s)	-	+

^(a) Different protons linked on molecular structures are marked as a, b, c, d, e and f, respectively.

^(b) Singlet, doublet, triplet, and multilet are abbreviated as s, d, t and m, respectively; coupling constants (J) are given hertz.

^(c) -, absence; +, presence.

^(d) Identified in organic extracts only. The NMR spectra of organic extracts were not showed in the present paper.

